ADVANCED HEALTHCARE MATERIALS
www.advhealthmat.de

Electroforming of Implantable Tubular Magnetic Microrobots for Wireless Ophthalmologic Applications

*George Chatzipirpiridis, Olgaç Ergeneman, Juho Pokki, Franziska Ullrich, Stefano Fusco, José A. Ortega, Kartik M. Sivaraman, Bradley J. Nelson, and Salvador Pané**

Retinal pathologies such as posterior uveitis (PU), age-related macular degeneration (AMD), or retinal vein occlusion (RVO) are among the leading causes of irreversible vision loss in elder adults.[1] Current strategies to treat these diseases include topical administration of drugs, intravitreal injections, laser surgery, or photodynamic therapy.[2] The efficacy of topically administered drops or ointments to the eye is poor due to their rapid excretion by lachrymal fluids before any substantial intraocular penetration can occur.[3] Moreover, drug delivery at the posterior segment of the eye using this approach is hampered by the presence of multiple physiological barriers.[4,5] Alternatively, intravitreal injections of drugs offer some advantages over topical administration, but they require regular doses leading to patient discomfort and side effects such as endophthalmitis, retinal detachment, hemorrhage, and infection.[1,3] Laser surgery is another type of therapy used and consists of inducing local coagulation of abnormal leaky blood vessels. However, this treatment entails collateral damage to adjacent neurosensory retina.[2] In contrast, photodynamic therapy is less harmful than laser surgery since it uses low light intensities. This treatment involves the injection of a photosensitizing agent intravenously. The drug is photochemically excited at the retinal vessels, thus triggering the blood-clotting cascade locally.[6] However, drugs used in this therapy are reported to cause some adverse effects.[7] All the above-mentioned methods are invasive, time consuming, and they are only applicable in the early stages of the disease.

Progress in micro- and nanotechnology has extensively contributed to the development of new strategies to mitigate the drawbacks displayed by current ocular therapies.[8–10] The use of nanoparticles, gels, drug-eluting contact lenses, and miniaturized implantable devices has been reported.[11] Indeed, recent years have seen advanced clinical trials and even commercialization of intravitreal implants such as Retisert (Bausch Lomb, Rochester, NY, USA) or the ones manufactured by SurModics, Inc (Eden Prairie, MN). Due to their proximity to the target area, these implants use a lower therapeutic load, which reduces the possibility of harmful side effects. Also, they are capable of sustained release of the drug over a long period of time, which minimizes the need for frequently repeated doses.[12] For example, Retisert implants are small polymeric tubes designed to release fluocinolone acetonide, a corticosteroid for treating PU, over 3 years. Despite improving visual acuity of the patients, these implants show some side effects such as increased intraocular pressure and cataract progression.[13] The I-vation (SurModics, Eden Prairie, MN) implant consists of a titanium helical coil coated with erodible films filled with triamcinolone acetonide to target diabetic macular edema (DME).[14] The main disadvantages of both implants include the initial surgery, as well as the removal surgery in case of adverse response or rejection of the implanted body.[15] Other implants such as Iluvien (pSivida) overcome the inconvenience of initial surgery. This implant is a small non-erodible polyimide tube that also contains fluocinolone acetonide.[16] Despite being sutureless injectable, once the tube is inserted, it is difficult to position precisely in the eye, and, in case of adverse reaction, surgery may be unavoidable.

Microrobots are proposed as implantable devices that can be controlled wirelessly and may, in the future, perform tasks such as targeted drug delivery, remote diagnostics, and minimally invasive surgery.[17–19] They can be operated in areas of the body that are currently difficult to access and precisely controlled beyond the limits of human dexterity. Development of these devices requires a co-ordination between diverse disciplines such as control systems, biomaterials, and microsystems. Due to the unfavorable scaling of energy sources at the microscale, power transmission to microrobots is one of the primary challenges.[20] The most favorable strategy would be to design these robots to harvest energy from their surroundings. Magnetic manipulation has emerged as a promising method in this regard because magnetic fields are capable of penetrating most materials with minimal interaction, and are nearly harmless to human beings. Magnetic fields have been successfully used to wirelessly manipulate microdevices of various sizes and shapes.[21,22]

In this paper, we present an implantable magnetic tubular microrobot for use in targeted drug delivery and minimally invasive surgery at the posterior segment of the eye. The tubular shape is preferred because it maximizes the volume of magnetic material that can fit into a 23-gauge needle and enables sutureless injections into the eye. Fabrication of tubular microstructures has been extensively investigated for several applications such as drug delivery, biosensing, microfluidics, and 3D cell microreactors.[23] Fabrication methods include rolling-up processes,[24] template-assisted atomic layer deposition,[25] spin forming,[26] or water-jet cutting.[27] However, these methods are either time consuming or do not produce the desired geometries of required dimensions. In contrast,

G. Chatzipirpiridis, Dr. O. Ergeneman, J. Pokki, F. Ullrich, S. Fusco, Dr. J. A. Ortega, Dr. K. M. Sivaraman, Prof. B. J. Nelson, Dr. S. Pané
Institute of Robotics & Intelligent Systems (IRIS)
ETH Zürich, Zurich, Switzerland
E-mail: vidalp@ethz.ch

DOI: 10.1002/adhm.201400256

© 2014 WILEY-VCH Verlag GmbH & Co. KGaA, Weinheim

electrochemical deposition (ED) methods offer a high level of tunability in shape, size, and chemical composition.[28] Moreover, ED is compatible with other micro and nanofabrication processes such as photolithography, replica molding, and colloidal lithography.[29] For example, electrodeposited nickel has been used to fabricate microrobots that can be wirelessly maneuvered in 3D space with a high degree of precision using magnetic fields. Wireless intraocular oxygen sensing has been demonstrated with this approach.[30]

In order to create tubular magnetic implants with relatively large amount of magnetic material, and controllable dimensions, we have developed an electrochemical method based on electroforming. This method is widely used in industry to manufacture complex macroscale shapes and surfaces.[31] The microtube was fabricated by electroforming galvanostatically cobalt–nickel (CoNi) on an aluminum wire as a sacrificial mandrel coated with a gold seed layer. A custom setup was designed (Figure S1, Supporting Information), and the fabrication steps are shown in **Figure 1**a. Smooth surface finishing was obtained with pulse deposition, while direct current deposition led to non-uniform pitted deposits (see Figure S3, Supporting Information). After the deposition, the aluminum wire was selectively etched to form a hollow lumen. Figure 1b,c show a CoNi tube and its cross-section with outer and inner diameters of 300 and 125 µm, respectively. The coating consists of 60% Co and exhibited a mixture of face-centered cubic, hexagonal-close-packed and amorphous structures (see Supporting Information). Using the same technology, microrobots with a sharp tip were also fabricated by electroforming CoNi on stainless steel needles at the same conditions (Figure 1d). The size of the devices was optimized for ophthalmic applications. **Figure 2** shows the microrobots on a chorioallantoic membrane (CAM) of a developing chicken embryo, in a 23-gauge-needle tip and on the fingertip. Despite cobalt and nickel being resistant to severe corrosive environments,[32] their ionic forms are reported to cause retinal cytotoxicity in trace concentrations.[33] To ensure their biocompatibility, the tubular implants were conformally coated by electropolymerization of polypyrrole (Ppy)–dodecylbenzenesulfonate (DBS) films (see Figure S4c and S4d, Supporting Information). We have recently shown that these Ppy coatings can be electrochemically modified to attenuate biofouling and cell adhesion.[34]

The CoNi tubes exhibited soft ferromagnetic behavior (**Figure 3**a) as can be seen from the hysteresis loops, and they were compared to commercially available hard ferromagnetic NdFeB cylinders, and stainless steel needles. CoNi cylinders showed the highest saturation magnetization and the lowest coercivity H_c. In general, for a binary alloy forming a solid solution, the dependence of its saturation magnetization (M_S) on its composition is unpredictable.[35] However, for our CoNi cylinders, one could consider that M_S varies linearly with the weight percent x of each element and is given by

$$M_{S,CoNi} = x_{Ni}M_{S,Ni} + x_{Co}M_{S,Co} \quad (1)$$

As $M_{S,Co}$ = 1.79 T and $M_{S,Ni}$ = 0.61 T, then $M_{S,\ CoNi} \approx$ 1.3 T, which is confirmed experimentally. Stainless steel is used widely for medical tools and devices due to its biocompatibility, durability, and strength. The stainless steel needles showed lower M_S and higher H_c with respect to CoNi. NdFeB cylinders showed values of magnetization closer to M_S for CoNi, and also high remanent magnetization and H_c. For wireless magnetic

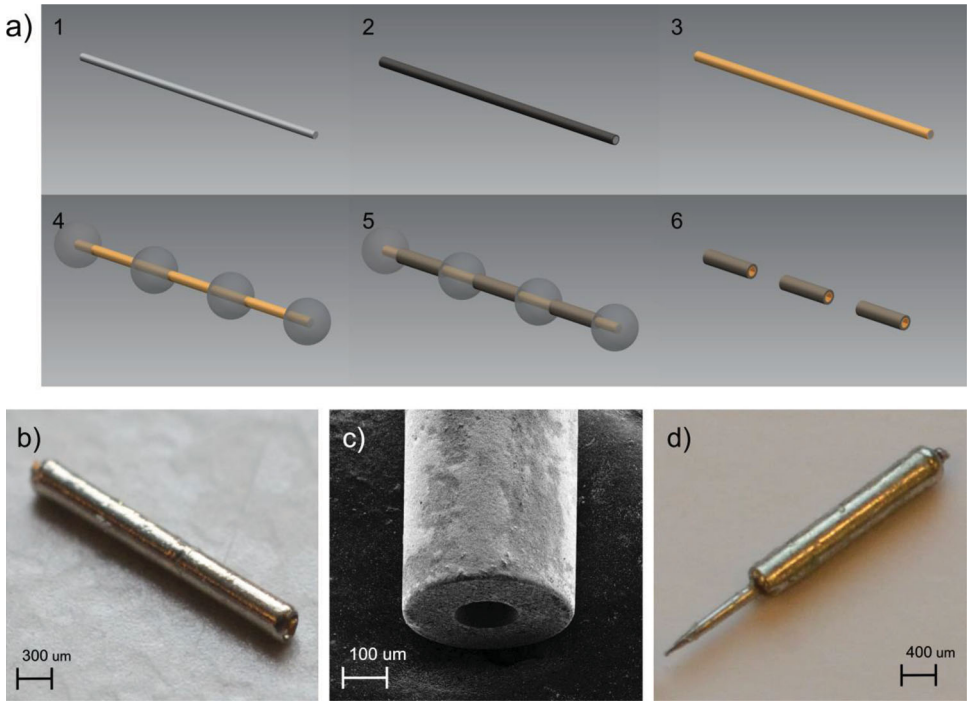

Figure 1. a) 1) Fabrication steps of magnetic microtubes starting with sacrificial aluminum wire; 2) palladization; 3) electroless gold plating; 4) lacquer spacers; 5) CoNi electroforming; 6) removal of the lacquer and selective etching of the sacrificial wire. b) CoNi microtube. c) SEM image of a CoNi tube. d) Electroformed CoNi on a stainless steel microneedle.

© 2014 WILEY-VCH Verlag GmbH & Co. KGaA, Weinheim
Adv. Healthcare Mater. **2014**,
DOI: 10.1002/adhm.201400256

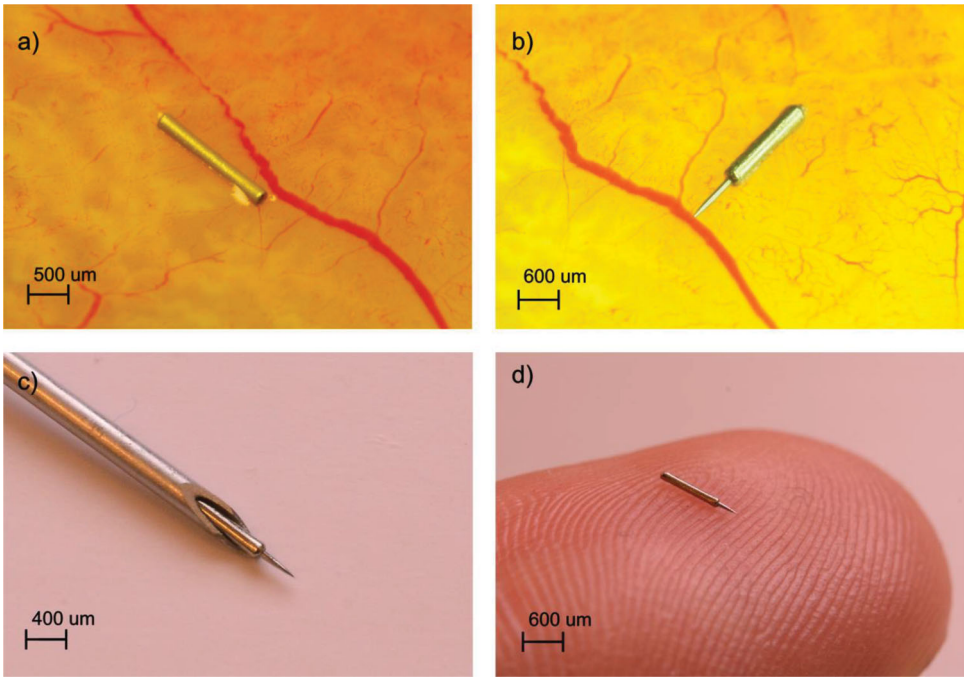

Figure 2. a) CoNi microtube on a chorioallantoic membranes (CAM) of a developing chicken embryo. b–d) CoNi stainless steel microneedle on a CAM, fitted in a 23-gauge needle, and on the tip of a finger, respectively.

manipulation, CoNi and NdFeB are among the best options due to their magnetic properties. If the applied magnetic field strength is lower than 3×10^4 A m^{-1}, NdFeB can provide preferable magnetization characteristics. CoNi exhibits the highest M_S and requires low magnetic fields to reach saturation. However, CoNi has superior durability and biocompatibility compared with NdFeB,[36] making it more attractive for medical applications.

To test their maneuverability, the CoNi microtubes were actuated with the OctoMag system, which enables

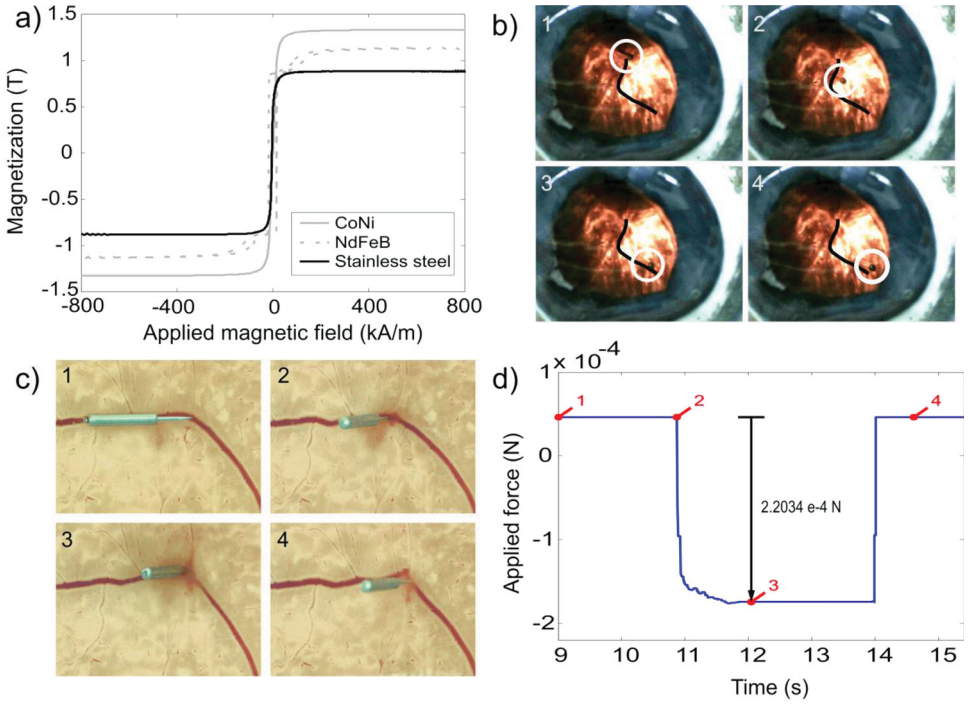

Figure 3. a) VSM measurements of magnetic cylinders. b) CoNi microtube steered along a vein in a porcine eye. c) Puncture sequence of a blood vessel in a chicken embryo and d) applied puncture forces, respectively.

© 2014 WILEY-VCH Verlag GmbH & Co. KGaA, Weinheim

ADVANCED HEALTHCARE MATERIALS
www.advhealthmat.de

www.MaterialsViews.com

five-degree-of-freedom (5-DOF) wireless magnetic control of a fully untethered microrobot (3-DOF position and 2-DOF pointing orientation).[21] Equations related to maneuvering soft ferromagnetic bodies can be found in the Supporting Information. CoNi microtubes with outer and inner diameters of 350 µm and 250 µm, respectively, and a length of 3.4 mm were prepared to test their control and steering with magnetic fields. The microtubes were first examined in silicon oil. Figure S5a,b (Supporting Information) show a microtube moving in a plane along the *X*–*Y* axes, and rotating around the *Y*-axes out of plane. Both experiments were performed with a field magnitude of 40 mT and a magnetic field gradient of 500 mT m^{-1} The resulting magnetization of the tubes under this field was calculated to be $M = 1.186$ T. The applied force was calculated as 7.54×10^{-5} N. Next, the microtubes were examined in porcine eyes. In Figure 3b, the photo sequence of a CoNi tube steered along a vein in a porcine eye is shown (see video in Supporting Information). The vein is marked with a black line. The stainless steel needles coated with CoNi were manipulated to perform puncture experiments in veins of CAMs of developing chicken embryos. Ophthalmologists have used these CAMs as a model system for studying photodynamic therapy and ocular angiogenesis.[37] Figure 3c,d depict, respectively, a puncture sequence and a plot of the applied force with respect to time corresponding to the sequence. The dots, from left to right, illustrate the applied force at each photo step (see video in Supporting Information). The offset force applied at the beginning maintains the microrobot at a stable position. Additional experiments manipulating vessels are provided as videos in the Supporting Information.

To evaluate the ability of intravitreal operations in vivo mobility experiments were conducted with the microtubes in rabbits eyes. New Zealand white rabbit breed (9-month-old females) was chosen for this study. The rabbit was anesthetized and its head was placed inside the workspace of the OctoMag, such that the studied eye is located in its center, as illustrated in **Figure 4**a. A microrobot was injected with a 23-gauge needle into the central vitreous humor of the eye and monitored with an ophthalmoscope with integrated camera. Magnetic torques and forces were applied to the intraocular microrobot and its rotational and translational mobility was analyzed for numerous frequencies and magnetic field magnitudes. It was observed that the intravitreal microrobot followed the applied rotating magnetic field with a time delay. The time delay between the rotating field and the microrobot is caused by the high viscosity of the vitreous humor, which acts as a damper on the microrobot. Figure 4b depicts the rotation of a microrobot around three axes at a field rotational frequency of 1 Hz in the vitreous humor of a living rabbit eye. A complete in vivo analysis of the microrobot's mobility and manipulability was conducted by Ullrich et al.[38] In vivo experiments in lapine eyes have demonstrated the wireless control of microrobots inside the vitreous. These experiments show the potential of this technology for applications in minimally invasive surgery.

Preliminary drug release studies were also conducted with the CoNi microtubes. An ideal drug delivery system (DDS)

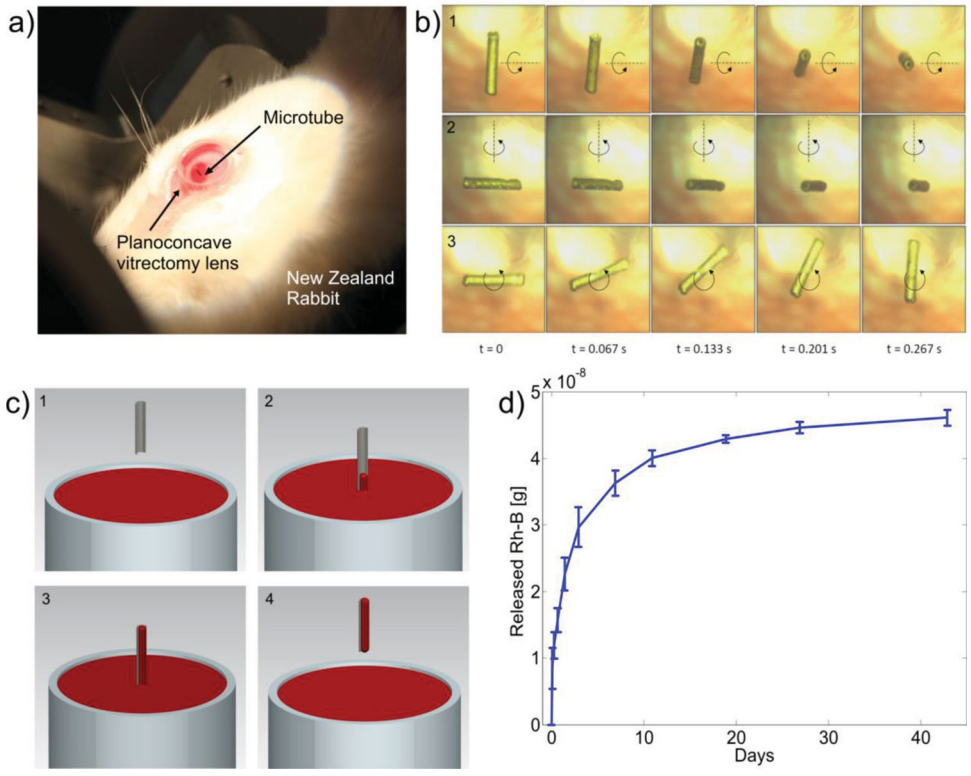

Figure 4. a) Rotation of a microrobot around three axes at a field rotational frequency of 1 Hz in the vitreous humor of a living rabbit eye. b) Anesthetized New Zealand rabbit with a microrobot inside the vitreous humor. c) Filling procedure of the microtubes. d) Release study of six microtubes over a period of 42 d. The error bars indicate the standard deviation.

© 2014 WILEY-VCH Verlag GmbH & Co. KGaA, Weinheim

DOI: 10.1002/adhm.201400256

delivers medication exclusively to the targeted part of the body in a programmable and controllable manner, thus limiting side effects due to systemic exposure. In this way, smaller drug quantities can be delivered more efficiently.[37] A non-erodible device, like the one presented here, acts as a "matrix" system, where diffusion of the drug can be controlled by the size of the device and the chemistry of the drug formulation.[39–41] However, filling the micron-sized tubes poses the challenge of loading them efficiently. As a proof of concept, we designed a method to load the microtubes using capillary forces. The microtubes were mounted in a custom setup and, by means of a micromanipulator, were positioned accurately until the base of the tube contacted the drug-containing solution (see Figure 4c). A video showing the filling procedure is provided as S9 (Supporting Information). This method minimizes the adsorption of filling material on the outer walls of the tube. Rhodamine B (Rh-B) was used as a model drug to fill the microtubes. Rh-B is a hydrophobic dye that has been used previously as a test molecule in intraocular dynamics.[42] Gelatin, a translucent, colorless solid substance, derived from collagen, and often used for drug delivery applications,[43,44] was employed as a degradable matrix to evaluate the loading and release of Rh-B from the microtubes. Figure 4d illustrates the release curve for a period of over a month. No significant release was observed after 42 d and the release was calculated to be 92%. The total loading of Rh-B inside the microtubes was determined as 5×10^{-8} g.

Magnetic microtubes are promising implantable devices not only for ophthalmic drug delivery at the posterior segment of the eye, but also for targeting other diseases in confined spaces of the human body. Many groups of body organs such as the circulatory or the brain systems have the potential to benefit from the technology considered in this manuscript.

Experimental Section

Electroforming of the CoNi Microtubes: CoNi cylinders were electroformed on a rotating sacrificial seed wire of aluminum (Goodfellow) with a Gamry potentiostat/galvanostat (Reference 3000). The electrolyte composition can be found in Table S2 (Supporting Information). A custom setup was constructed enabling deposition on a wire length of 83 mm. The wire was held on one side with a metal chuck (Albrecht) and a pull-spring on the other end to maintain constant tension. The counter electrode was a 83 mm × 30 mm sulfurized nickel sheet. CoNi was pulse plated galvanostatically with a current density of –70 mA cm^{-2} and a duty cycle of 50% with $t_{ON} = t_{OFF} = 500$ ms. Throughout the entire deposition, the wire was rotated at 100 rpm by a DC motor. The electrolyte overflowed from the sides and was collected in a second tank, filtered, and circulated back to the deposition tank with a peristaltic pump (Verdeflex S40). The composition of the electrolyte and the plating conditions can be found in the Supporting Information. Prior to the electrodeposition, the aluminum wire was rinsed sequentially in acetone, isopropanol, and Millipore Milli-Q water for 1–2 min each. In order to remove the native aluminum oxide layer, the wire was immersed in a KOH solution (100 mL, 2.5 g L^{-1}) at 70 °C for 1 min. The aluminum surface was activated by dipping the wire for 1 min at room temperature in a solution containing palladium(II) chloride (0.5 g L^{-1}) and hydrochloric acid (1 mL L^{-1} of HCl 35%). Subsequently, the wire was immersed in a cyanide-based electroless gold solution (Transene Inc.) for 20 min at 90 °C. Microrobots with a sharp tip were fabricated with the setup mentioned earlier and CoNi was electroformed on a stainless steel needle. The needles were connected to the chuck and immersed in the electrolyte. Prior to the deposition, the needles were sequentially rinsed with acetone, isopropanol, Millipore Milli-Q water, and the tip was covered with a lacquer drop to avoid deposition at the sharp tip. All electrodeposition parameters were the same as for the aluminum wire and CoNi was electrodeposited on stainless steel needles.

Coatings for CoNi Cylinders: Ppy was electrodeposited from a three-electrode single-compartment cell using a Ag/AgCl reference electrode and a platinized titanium counter electrode. Prior to the electrodeposition, the Au-coated CoNi cylinders were cleaned by sequentially washing with acetone, isopropyl alcohol, and Millipore Milli-Q water. A current density of 1 mA cm^{-2} was applied using the Gamry Reference 3000. The electrolyte consisted of doubly distilled pyrrole monomer (0.1 mol L^{-1}) and sodium dodecylbenzenesulfonate (0.1 mol L^{-1}). All experiments were carried out in a nitrogen atmosphere and under quiescent conditions at room temperature.

Characterization: The morphology of the microstructures was observed by optical microscopy and SEM in a Zeiss Ultra 55. The composition was determined by energy-dispersive X-ray spectroscopy (EDX). The structure of the CoNi was obtained by X-ray diffraction (XRD) using a Philips X'Pert diffractometer using the Cu-Kα radiation in the 30–70° 2θ range (0.03° step size, 10 s holding time). Room-temperature magnetic hysteresis curves of samples were recorded in a Princeton Measurement Corp. MicroMag 3900 vibrating sample magnetometer to a maximum applied magnetic field of 1 T.

Manipulation: The microtubes were actuated with the OctoMag,[21] a five-degree-of-freedom electromagnetic system with stationary electromagnets and soft magnetic cores, operated within their linear magnetization region. The microtubes were examined in silicon oil (Wacker, AK 1000), in ex vivo porcine eyes and in vivo lapine eyes. The porcine eyes were purchased from a local abattoir. They were stored at 5 °C and were used within 5 h. The eyes were fixed to a rubber support, and their cornea, iris, and lens were carefully removed to expose the vitreous humor (Figure S7, Supporting Information). Transscleral illumination through the optic nerve region was applied for high contrast imaging. The experiments were conducted with the vitreous humor in the eye globe. The magnetic microneedles were manipulated in CAMs of developing chicken embryos prepared as described in ref. [45] More detailed CAM preparation can be found in the Supporting Information. In vivo mobility experiments were conducted with New Zealand white rabbit breed, 9-month-old females. The rabbit was anesthetized and its head was placed inside the workspace of the OctoMag. The protocols concerning animal housing, treatment, and monitoring were approved by the Swiss Veterinary Office according to the Swiss decree on animal protection.[46] This study was undertaken in cooperation with ophthalmologists from the University Hospital Bern and the Veterinary Hospital Zurich.

Drug Release Studies with CoNi Microtubes: A solution containing 625 mg L^{-1} of Rh-B and 24 g L^{-1} of gelatin was prepared and six microtubes with an inner diameter of 125 µm and a length of 3 mm were filled. Figure 4c illustrates the filling procedure of the microtubes. The microtubes were subsequently cooled at 5 °C for 6 h to solidify the gelatin. In vitro release of Rh-B was monitored by evaluating the fluorescence intensity (TECAN infinite 200 plate reader, Switzerland) at the emission wavelength of 625 nm (excitation wavelength, 540 nm). Each cylinder was placed in a separate well with 250 µL of Millipore Milli-Q water in a six-well transparent multiwall plate. The laser beam height was adjusted in order to measure at the center of the solution and multiple measurements were taken for each well. At defined times, measurements were taken and Millipore Milli-Q water was replaced with fresh solution in order to mimic a perfect sink solution. The total loading of Rh-B inside the tube was determined from two microtubes, which were filled without solidifying the gelatin and, immediately dissolving them after filling.

Supporting Information

Supporting Information is available from the Wiley Online Library or from the author

© 2014 WILEY-VCH Verlag GmbH & Co. KGaA, Weinheim

Acknowledgements

The authors thank Dr. Eva Pellicer and Prof. Jordi Sort for providing the data corresponding to the composition and the crystal structure of the CoNi microtubes, Michael Karth for the use of the Verdeflex peristaltic pump, and Prof. P. Vögeli for the use of their incubator. The authors thank the FIRST lab for their technical support. This study was funded by the NCCR Co-Me of the Swiss National Science Foundation. Funding for this research was also provided by the European Research Council Advanced Grant "Microrobotics and Nanomedicine (BOTMED)".

Received: May 14, 2014
Published online:

[1] D. H. Geroski, H. F. Edelhauser, *Invest. Ophthalmol. Vis. Sci.* **2000**, *41*, 964.
[2] U. M. Schmidt-Erfurth, G. Richard, A. Augustin, W. G. Aylward, F. Bandello, B. Corcòstegui, J. Cunha-Vaz, A. Gaudric, A. Leys, R. O. Schlingemann, *Acta Ophthalmol. Scand.* **2007**, *85*, 486.
[3] C. Schultz, J. Breaux, J. Schentag, D. Morck, *Clin. Exp. Optom.* **2011**, *94*, 212.
[4] T. R. Thrimawithana, S. Young, C. R. Bunt, C. Green, R. G. Alany, *Drug Discovery Today* **2011**, *16*, 270.
[5] G. Velez, S. M. Whitcup, *Br. J. Ophthalmol.* **1995**, *83*, 1225.
[6] X.-X. Zhou, Y.-P. Song, Y.-X. Zhao, J.-G. Wu, in *Advances in Ophthalmology*, (Ed: S. Rumelt), InTech, China **2012**, Ch. 22.
[7] M. Berdugo, R. A. Bejjani, F. Valamanesh, M. Savoldelli, J.-C. Jeanny, D. Blanc, H. Ficheux, A. Scherz, Y. Salomon, D. BenEzra, F. Behar-Cohen, *Invest. Ophthalmol. Vis. Sci.* **2008**, *49*, 1633.
[8] K. Mathieson, J. Loudin, G. Goetz, P. Huie, L. Wang, T. I. Kamins, L. Galmabos, R. Smith, J. S. Harris, A. Sher, D. Palanker, *Nat. Photonics* **2012**, *6*, 391.
[9] P.-J. Chen, S. Saati, R. Varma, M. S. Humayun, Y. C. Tai, *J. Microelectromech. Syst.* **2010**, *4*, 721.
[10] D. D. Zhou, R. J. Greenberg, *Front Biosci.* **2005**, *10*, 166.
[11] A. L. Weiner, B. C. Gilger, *Vet. Ophthalmol.* **2010**, *13*, 395.
[12] C. L. Stevenson, J. T. Santini, R. Langer, *Adv. Drug Delivery Syst.* **2012**, *64*, 1590.
[13] G. J. Jaffe, D. Martin, D. Callanan, P. A. Pearson, B. Levy, T. Comstock, *Ophthalmology* **2006**, *113*, 1020.
[14] J. B. Christoforidis, S. Chang, A. Jiang, J. Wang, C. M. Cebulla, *Med. Inflammation* **2013**, *8*, 126463.
[15] E. Lavik, M. H. Kuehn, Y. H. Kwon, *Eye* **2011**, *25*, 578.
[16] M. Sanford, *Drugs* **2013**, *73*, 187.
[17] B. J. Nelson, I. K. Kaliakatsos, J. J. Abbott, *Annu. Rev. Biomed. Eng.* **2010**, *12*, 55.
[18] A. A. Solovev, W. Xi, D. H. Gracias, S. M. Harazim, C. Deneke, S. Sanchez, O. G. Schmidt, *ACS Nano* **2012**, *6*, 1751.
[19] W. Xi, A. A. Solovev, A. N. Ananth, D. H. Gracias, S. Sanchez, O. G. Schmidt, *Nanoscale* **2013**, *5*, 1294.
[20] J. J. Abbott, Z. Nagy, F. Beyeler, B. J. Nelson, *IEEE Rob. Autom. Mag.* **2007**, *14*, 92.
[21] M. Kummer, J. J. Abbott, B. E. Kratochvil, R. Borer, A. Sengul, B. J. Nelson, *IEEE Trans. Robot.* **2010**, *26*, 1006.
[22] L. Zhang, K. E. Peyer, B. J. Nelson, *Lab Chip* **2010**, *10*, 2203.
[23] S. M. Harazim, W. Xi, C. K. Schmidt, S. Sanchez, O. G. Schmidt, *J. Mater. Chem.* **2012**, *22*, 2878.
[24] O. G. Schmidt, K. Eberl, *Nature* **2001**, *410*, 168.
[25] K. Pitzschel, J. Bachmann, J. M. Montero-Moreno, J. Escrig, D. Görlitz, K. Nielsch, *IOP Nanotechnol.* **2012**, *23*, 495718.
[26] Y. Tang, Y. Chi, J. Ch. Chen, X. X. Deng, L. Liu, X. K. Liu, Zh. P. Wan, *Int. J. Mach. Tools Manuf.* **2007**, *47*, 1059.
[27] H. Orbanic, B. Jurisevic, D. Kramar, M. Grah, M. Junkar, *Proc. Inst. Mech. Eng C: J. Mech. Eng. Sci.* **2006**, *220*, 1697.
[28] W. Ruythooren, K. Attenborough, S. Beerten, P. Merken, J. Fransaer, E. Beyne, C. Van Hoof, J. De Boeck, J. P. Celis, *J. Micromech. Microeng.* **2000**, *10*, 101.
[29] D. Wei, in *Electrochemical Nanofabrication,* (Ed: D. Wei), Pan Stanford Publishing, Singapore **2012**, Ch. 1.
[30] O. Ergeneman, G. Chatzipirpiridis, J. Pokki, M. M. Toro, G. A. Sotiriou, S. Medina-Rodrígez, J. F. Sánchez, A. Fernandéz-Gutiérrez, S. Pané, B. J. Nelson, *IEEE Trans. Biomed. Eng.* **2011**, *59*, 3104.
[31] T. Hart, A. Watson, *Met. Finish* **1999**, *97*, 388.
[32] J. R. Davis, *Nickel, Cobalt, and Their Alloys,* (Ed: ASM International Handbook Committee), ASM International, Materials Park, OH **2000**.
[33] W. Apel, D. Stark, A. Stark, S. O'Hagan, J. Ling, *Doc. Ophthalmol.* **2013**, *126*, 69.
[34] K. M. Sivaraman, B. Özkale, O. Ergeneman, T. Lühmann, G. Fortunato, M. A. Zeeshan, B. J. Nelson, S. Pané, *Adv. Healthcare Mater.* **2013**, *2*, 591.
[35] B. D. Cullity, C. D. Graham, *Introduction to Magnetic Materials,* (Ed: IEEE Press Editorial Board), IEEE Press and John Wiley & Sons, New Jersey **2009**, Ch. 4.
[36] M. Hopp, S. Rogaschewski, Th. Groth, *J. Mater. Sci: Mater. Med.* **2003**, *14*, 335.
[37] I. Fleming, M. Balicki, J. Koo, I. Iordachita, B. Mitchell, J. Handa, G. Hager, R. Taylor, *Med. Image Comput. Comput. Assist. Interv.* **2008**, *5242*, 543.
[38] F. Ullrich, C. Bergeles, J. Pokki, O. Ergeneman, S. Erni, G. Chatzipirpiridis, S. Pané, C. Framme, B. J. Nelson, *Invest. Ophthalmol. Vis. Sci.* **2013**, *54*, 4.
[39] D. Y. Artifin, Y. L. Lee, C. H. Wang, *Adv. Drug Delivery Rev.* **2006**, *58*, 1274.
[40] Y. Fu, W. J. Kao, *Expert Opin. Drug Delivery* **2010**, *7*, 429.
[41] N. Rajgor, M. Patel, V. H. Bhaskar, *Syst. Rev. Pharm.* **2011**, *2*, 91.
[42] R. Guss, F. Johnson, D. Maurice, *Invest. Ophthalmol. Vis. Sci.* **1984**, *25*, 758.
[43] L. Di Silvio, R. G. Courteney-Harris, S. Downes, *J. Mater. Sci.: Mater. Med.* **1994**, *5*, 819.
[44] S. Young, M. Wong, Y. Tabata, A. G. Mikos, *J. Controlled Release* **2005**, *109*, 256.
[45] T. Leng, J. M. Miller, K. V. Bilbao, D. V. Palanker, P. Huie, M. S. Blumenkranz, *Retina* **2004**, *24*, 427.
[46] The Federal Authorities of the Swiss Confederation. Tierschutzverordnung. Available at: http://www.admin.ch/ch/d/sr/455_1/index.html (accessed: September, **2012**).

© 2014 WILEY-VCH Verlag GmbH & Co. KGaA, Weinheim